5266 *Inorg. Chem.* **1999,** *38,* 5266−5276

Tetranuclear Copper(II) and Nickel(II) Cluster Complexes Derived by Self-Assembly from a Series of Tetradentate Diazine Ligands: Structural and Magnetic Studies

Craig J. Matthews,[†] Karen Avery,[†] Zhiqiang Xu,[†] Laurence K. Thompson,[*,†] Liang Zhao,[†] David O. Miller,[†] Kumar Biradha,[‡] Karen Poirier,[‡] Michael J. Zaworotko,[‡,||] Claire Wilson,[§] Andrés E. Goeta,[§] and Judith A. K. Howard[§]

Departments of Chemistry, Memorial University of Newfoundland, St. John’s, Newfoundland,
A1B 3X7, Canada, St. Mary’s University, Halifax, Nova Scotia B3H 3B3, Canada, and
University of Durham, Durham DH1 3LE, United Kingdom

Received May 24, 1999

A series of tetranuclear copper(II) and nickel(II) complexes is described, all of which form by a strict self-assembly process involving just a single ligand and the metal salt. The ligands POAP, POAPZ, PZOAP, and 6POAP contain terminal pyridine and pyrazine residues bound to a central flexible diazine subunit (N−N) and contain two potentially bridging groups (alkoxo and diazine). In all cases but one the metals are linked by alkoxo oxygens alone, forming essentially square $[M_4(\mu_2\text{-}O)_4]$ clusters. A rectangular copper(II) complex $[Cu_4(\mu_2\text{-}N_2)_2(\mu_2\text{-}O)_2]$ involves a mixture of two alkoxo and two diazine bridges. The square Cu_4O_4 clusters exhibit ferromagnetic coupling between the metal centers, associated with the orthogonal arrangement of magnetic orbitals, while for the Ni_4O_4 clusters the nickel(II) centers are coupled antiferromagnetically. The $[Cu_4(\mu_2\text{-}N_2)_2(\mu_2\text{-}O)_2]$ cluster exhibits strong antiferromagnetic coupling through a trans Cu(N-N)Cu bridging arrangement, typical for systems of this sort. X-ray structures are reported for $[Cu_4(POAP\text{-}H)_4(H_2O)_2](NO_3)_4\cdot 4H_2O$ (**2**), $[Cu_4(POAPZ\text{-}H)_4(H_2O)](NO_3)_4\cdot 3H_2O$ (**3**), $[Cu_4(6POAP\text{-}H)_4](ClO_4)_4$ (**4**), $[Cu_4(PZOAP\text{-}H)_4](NO_3)_4\cdot 3H_2O$ (**5**), $[Ni_4(POAP\text{-}H)_4(H_2O)_4](NO_3)_4\cdot 8H_2O$ (**6**), and $[Ni_4(PZOAP\text{-}H)_4(H_2O)_4](ClO_4)_4\cdot 5H_2O$ (**9**). **2** crystallized in the monoclinic system, space group $C2/c$, with $a = 20.479(3)$ Å, $b = 14.920(2)$ Å, $c = 19.671(3)$ Å, $\beta = 90.591(4)°$, and $Z = 8$. **3** crystallized in the monoclinic system, space group $P2_1/c$, with $a = 14.12(1)$ Å, $b = 14.116(3)$ Å, $c = 29.043(4)$ Å, $\beta = 94.50(3)°$, and $Z = 4$. **4** crystallized in the monoclinic system, space group $C2/c$, with $a = 22.646(4)$ Å, $b = 25.842(5)$ Å, $c = 12.349(5)$ Å, $\beta = 110.34(2)°$, and $Z = 4$. **5** crystallized in the monoclinic system, space group $P2/n$, with $a = 14.3573(4)$ Å, $b = 10.8910(6)$ Å, $c = 20.5360(10)$ Å, $\beta = 96.975(4)°$, and $Z = 4$. **6** crystallized in the triclinic system, space group $P\bar{1}$, with $a = 12.0509(6)$ Å, $b = 12.7498(6)$ Å, $c = 23.1208$ Å, $\alpha = 93.1050(10)°$, $\beta = 100.1500(10)°$, $\gamma = 108.5050(11)°$, and $Z = 2$. **9** crystallized in the orthorhombic system, space group $Pbcn$, with $a = 14.368(4)$ Å, $b = 25.469(7)$ Å, $c = 18.479(5)$ Å, and $Z = 4$.

Introduction

The design of high nuclearity transition metal clusters with novel magnetic properties is a major goal of current research in the area of nanoscale materials. The size of large polymetallic clusters is difficult to control, and these systems are invariably obtained serendipitously through self-assembly reactions. A significant amount of control can be exerted over the formation of relatively low nuclearity molecular clusters ($<M_6$) by the use of polyfunctional and polytopic ligands with well defined and appropriately positioned coordination pockets. Cu_4, Cu_6, and Cu_8 complexes have been synthesized by the use of polyphthalazine ligands with fused and polypodal ligand fragments.[1,2] Transition metal template cyclizations have successfully produced many tetranuclear Mn_4,[3,4] Ni_4,[5−8] Cu_4,[9−12] and Zn_4[13,14] complexes, in which the metal ions are bridged exclusively by oxygen donor groups. The size of the macrocyclic ring can be modified by adjustments of chelate ring sizes, and with smaller chelate rings macrocyclic ligands accommodating six metals (Cu_6, Ni_6) can be produced,[15,16] and in the copper

---

[*] Corresponding author. Fax: 709-737-3702. E-mail: lthomp@morgan.ucs.mun.ca.

[†] Memorial University.

[‡] St. Mary’s University.

[§] University of Durham.

[||] Present address: Department of Chemistry, University of South Florida, Tampa, FL 33620-5250.

(1) Tandon, S. S.; Mandal, S. K.; Thompson, L. K.; Hynes, R. C. *Inorg. Chem.* **1992**, *31*, 2215.

(2) Zhang, Y.; Thompson, L. K.; Bridson, J. N.; Bubenik, M. *Inorg. Chem.* **1995**, *34*, 5870.

(3) McKee, V.; Sheppard, W. B. *J. Chem. Soc., Chem. Commun.* **1985**, 158.

(4) McKee, V.; Tandon, S. S. *J. Chem. Soc., Chem. Commun.* **1988**, 1334.

(5) Edwards, A. J.; Hoskins, B. F.; Kachab, E. H.; Markewiecz, A.; Murray, K. S.; Robson, R. *Inorg. Chem.* **1992**, *31*, 3585.

(6) Bell, M.; Edwards, A. J.; Hoskins, B. F.; Kachab, E. H.; Robson, R. *J. Am. Chem. Soc.* **1989**, *111*, 3603.

(7) Nanda, K. K.; Venkatsubramanian, K.; Majumdar, D.; Nag, K. *Inorg. Chem.* **1994**, *33*, 1581.

(8) Mohanta, S.; Nanda, K. K.; Werner, R.; Haase, W.; Mukherjee, A. K.; Dutta, S. K.; Nag, K. *Inorg. Chem.* **1997**, *36*, 4656.

(9) McKee, V.; Tandon, S. S. *J. Chem. Soc., Chem. Commun.* **1988**, 385.

(10) McKee, V.; Tandon, S. S. *Inorg. Chem.* **1989**, *28*, 2901.

(11) KcKee, V.; Tandon, S. S. *J. Chem. Soc., Dalton Trans.* **1991**, 221.

(12) Sakiyama, H.; Motoda, K.-I.; Ōkawa, H. *Chem. Lett.* **1991**, 1133.

(13) Grannas, M. J.; Hoskins, B. F.; Robson, R. *J. Chem. Soc., Chem. Commun.* **1990**, 1644.

(14) Grannas, M. J.; Hoskins, B. F.; Robson, R. *Inorg. Chem.* **1994,** *33*, 1071.

(15) Tandon, S. S.; Thompson, L. K.; Bridson, J. N. *J. Chem. Soc., Chem. Commun.* **1992**, 911.

(16) Tandon, S. S.; Thompson, L. K.; Bridson, J. N.; Benelli, C. *Inorg. Chem.* **1995**, *34*, 5507.

10.1021/ic990598f CCC: $18.00

case association between the rings produces spin coupled, dodecanuclear systems.

Controlling the nuclearity for clusters of large numbers of metals is very difficult, and requires an ingenious approach to the design of a single ligand. A more practical approach is based on the propensity of metal ions, given the right coordination environment, to self-assemble into a cluster. This occurs readily with simple bidentate ligands, which do not fully satisfy the coordination requirements of a single metal, and the vacant coordination sites are filled by spare donor fragments from a neighboring subunit as the overall cluster forms in a self-assembly process. Beta-diketones,[17] and pyridonates[18−20] have successfully been used, usually in conjunction with carboxylate bridging fragments or hydroxide, oxide or methoxide, which are produced accidentally during the reaction, to fulfill the coordination requirements of the homo- or hetero-metallic cluster. Nuclearities of four and higher have been produced in this fashion, but with little or no control over the reaction outcome. A large Fe_{12}[21] ring involving methoxide and carboxylate bridges, and a Cu_8[22] ring involving pyrazolate and hydroxide bridges, illustrate the subtle balance of the coordination algorithms of the metals and the coordination environments presented by the ligands, leading to molecular cluster species rather than polymers, and the fact that the outcome of the self-assembly process is impossible to predict.

"Polytopic" ligands, with well defined and appropriately separated coordination compartments, in principle have a better chance of control over the outcome of a self-assembly process to produce a cluster with a predefined nuclearity. Diazine ligands, e.g., pyridazines, phthalazines, pyrazoles, triazoles, etc. have a N_2 dinucleating fragment, which can provide a coordination focus for pairs of metal centers. Molecular $Cu(I)_4$[23] and $Ag(I)_9$[24] grids have been successfully produced with the ligands 3,6-bis(2′-pyridyl) pyridazine and 6,6′-bis[2-(6-methylpyridyl)]-3,3′-bipyridazine, respectively, in which the rigid, linear, polytopic ligands arrange themselves in two groups of two and three respectively, above and below the metallic planar grids. The coordination requirements of the planar arrangements of tetrahedral metal centers are exactly matched by the arrangement of the coordination pockets of the ligands. A planar $Cu(II)_4$ cluster with a tetradentate diazine (N_2) ligand[25] and tetrahedral $Cu(II)_4$ clusters with tetradentate triazolate[26] and pyrazolate[27] ligands with (N_2) bridges are also formed by self-assembly processes. A similar self-assembly produces a pseudo-square arrangement of four Co(II) centers with a bicompartmental bis-(bipyridyl)-pyrimidine ligand, in which the metals are bridged by pyrimidine groups.[28] Intramolecular antiferromagnetic coupling was reported for this system.[29]

Scheme 1

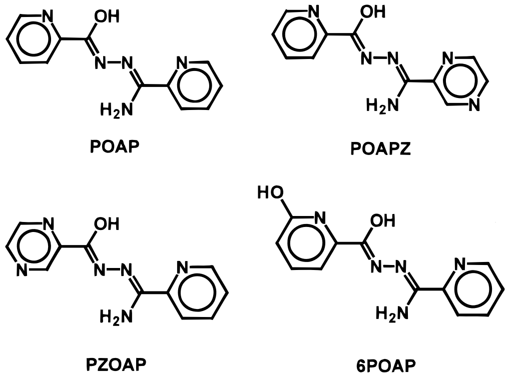

Within the framework of a self-assembly strategy we have developed a series of ligands that incorporate two different dinucleating fragments, alkoxo and diazine, which are both well-known to bridge metals and propagate spin coupling. The ligands POAP (formerly PHAAP), POAPZ, PZOAP, and 6POAP (Scheme 1) contain the saturated diazine N_2 fragment, which has been shown previously to act as a flexible bridge, with single bond character, and leads to a variety of exchange situations in its dicopper(II) complexes, where magnetic coupling is linearly dependent on the rotational angle of the copper magnetic planes about the N-N bond,[30,31] with ferromagnetic behavior at low rotational angles and antiferromagnetic behavior at large angles.

In this report the structural features and properties of the complexes $[Cu_4(POAP\text{-}H)_4(H_2O)_2](ClO_4)_4\cdot 4H_2O$ (**1**), $[Cu_4(POAP\text{-}H)_4(H_2O)_2]\ (NO_3)_4\cdot 4H_2O$ (**2**), $[Cu_4(POAPZ\text{-}H)_4(H_2O)](NO_3)_4\cdot 3H_2O$ (**3**), $[Cu_4(6POAP\text{-}H)_4](ClO_4)_4$ (**4**), $[Cu_4(PZOAP\text{-}H)_4](NO_3)_4\cdot 3H_2O$ (**5**), $[Ni_4(POAP\text{-}H)_4(H_2O)_4]\ (NO_3)_4\cdot 8H_2O$ (**6**), $[Ni_4(POAP\text{-}H)_4Cl(H_2O)_3]Cl_3\cdot 10.5H_2O$ (**7**), $[Ni_4(POAPZ\text{-}H)_4(H_2O)_4](ClO_4)_4\cdot 3H_2O$ (**8**), and $[Ni_4(PZOAP\text{-}H)_4(H_2O)_4]\ (ClO_4)_4\cdot 5H_2O$ (**9**) are reported. In general, square M_4O_4 clusters are formed, but in one unique case (**2**) a rectangular cluster results, with alternating Cu−O−Cu and Cu-N_2-Cu bridges. In all cases the metal centers are spin coupled within the cluster frameworks, with the Cu_4O_4 systems exhibiting weak ferromagnetic exchange, and the $Cu_4O_2(N_2)_2$ and Ni_4O_4 systems exhibiting antiferromagnetic exchange.

Experimental Section

Physical Measurements. Infrared spectra were recorded as Nujol mulls using a Mattson Polaris FTIR instrument. UV/VIS spectra were recorded in the solid state (mull transmittance) and solution using a Cary 5E spectrometer. Microanalyses were carried out by Canadian Microanalytical Service, Delta, Canada. Room-temperature magnetic susceptibilities were measured by the Faraday method using a homemade magnetometer comprising a Mettler ME21 microbalance and Cahn 0.8 T permanent magnet, fitted with Faraday pole caps; and variable temperature magnetic data (4−300 K) were obtained using a Quantum Design MPMS5S SQUID magnetometer with field strengths in the range of 0.1 to 1.0 T. Samples were prepared in gelatin capsules, mounted inside straws, and then fixed to the end of the sample transport rod. Background corrections for the sample holder assembly were applied.

---

(17) Halcrow, M. A.; Sun, J.-S.; Huffman, J. C.; Christou, G. *Inorg. Chem.* **1995**, *34*, 4167.
(18) Wang, S. *Inorg. Chem.* **1991**, *30*, 2252.
(19) Winpenny, R. E. P. *Comments Inorg. Chem.* **1999,** *20*, 233.
(20) Parsons, S.; Winpenny, R. E. P. *Acc. Chem. Res.* **1997**, *30*, 89.
(21) Taft, K. L.; Lippard, S. J. *J. Am. Chem. Soc.* **1990**, *112*, 9629.
(22) Ardizzoia, G. A.; Angaroni, M. A.; La Monica, G.; Cariati, F.; Moret, M.; Masciocchi, N. *J. Chem. Soc., Chem. Commun.* **1990**, 1021.
(23) Youinou, M.-T.; Rahmouni, N.; Fischer, J.; Osborn, J. A. *Angew. Chem., Int. Ed. Engl.* **1992**, *31*, 733.
(24) Baxter, P. N. W.; Lehn, J.-M.; Fischer, J.; Youinou, M.-T. *Angew. Chem., Int. Ed. Engl.* **1994**, *33*, 2284.
(25) Van Koningsbruggen, P. J.; Müller, E.; Haasnoot, J. G.; Reedijk, J. *Inorg. Chim. Acta*, **1993,** *208*, 37.
(26) Bencini, A.; Gatteschi, D.; Zanchini, C.; Haasnoot, J. G.; Prins, R.; Reedijk, J. *J. Am. Chem. Soc.* **1987**, *109*, 2926.
(27) Zhang, H.; Fu, D.; Ji, F.; Wang, G.; Yu, K.; Yao, T. *J. Chem. Soc., Dalton Trans.* **1996**, 3799.
(28) Hanan, G. S.; Volkmer, D.; Ulrich, S. S.; Lehn, J.-M.; Baum, G.; Fenske, D. *Angew. Chem., Int. Ed. Engl.* **1997**, *36*, 1842.
(29) Waldmann, O.; Hassmann, J.; Müller, P.; Hanan, G. S.; Volkmer, D.; Schubert, U. S.; Lehn, J.-M. *Phys. Rev. Lett.* **1997**, *78*, 3390.
(30) Xu, Z.; Thompson, L. K.; Miller, D. O. *Inorg. Chem.* **1997**, *36*, 3985.
(31) Thompson, L. K.; Xu, Z.; Goeta, A. E.; Howard, J. A. K.; Clase, H. J.; Miller, D. O. *Inorg. Chem.* **1998**, *37*, 3217.

Synthesis of Ligands and Complexes. POAP and POAPZ were synthesized by published procedures.[32] PZOAP and 6POAP were synthesized according to the following general procedure.

The methyl ester of imino-picolinic acid was prepared in situ by reaction of 2-cyanopyridine (2.2 g, 22 mmol) with sodium methoxide solution, produced by dissolving sodium metal (0.050 g, 2.2 mmol) in dry methanol (50 mL). The appropriate carboxylic acid hydrazide (22 mmol) (prepared from the reaction of methyl 2-pyrazine carboxylate (PZOAP) or 6-hydroxy methyl-2-pyridine carboxylate (6POAP) with hydrazine hydrate in methanol) was added to the above solution and the mixture refluxed for 24 h. Yellow powders were obtained, which were filtered off, washed with methanol, and then diethyl ether and dried under vacuum. Yields: PZOAP (74%), 6POAP (72%).

POAP. Pale yellow powder (mp 215−217 °C). ^{1}H NMR (300 MHz, DMSO-d_6, 25 °C): 8.68 (m, 1H, Ar), 8.60 (m, 1H, Ar), 8.21 (m, 1H, Ar), 8.18 (m, 1H, Ar), 8.03 (m, 1H, Ar), 7.90 (m, 1H, Ar), 7.61 (m, 1H, Ar), 7.48 (m, 1H, Ar), 7.04 (br s, 2H, NH_2). Mass spectrum (major mass peaks, *m*/*z*): 241(M), 224, 223 (M − NH_3 and M − H_2O, respectively), 194, 163, 107, 79. IR (Nujol mull, cm^{-1}): 3305 (w), 3167 (w) (νNH_2); 1667 (s) ($\nu C{=}O$); 1620 (m) ($\nu C{=}N$); 996 (m) (νpy). Anal. Calcd for $C_{12}H_{11}N_5O$: C, 59.75; H, 4.60; N, 29.21. Found: C, 59.73; H, 4.58; N, 29.34.

POAPZ. Pale yellow powder (mp 238−241 °C). ^{1}H NMR (300 MHz, DMSO-d_6, 25 °C): 9.33 (d, 1H, Ar), 8.69 (m, 3H, Ar), 8.04 (m, 2H, Ar), 7.63 (m, 1H, Ar), 7.10 (br s, 2H, NH_2). Mass spectrum (major mass peaks, *m*/*z*): 242 (M), 225, 224 (M − NH_3 and M − H_2O, respectively), 194, 163, 107, 79. IR (Nujol mull, cm^{-1}): 3415 (w), 3309 (w) (νNH_2); 3273−3210 (w) (νNH_2); 1666 (s) ($\nu C{=}O$); 1613 (m) ($\nu C{=}N$); 996 (m) (νpy). Anal. Calcd for $C_{11}H_{10}N_6O$: C, 54.54; H, 4.16; N, 34.69. Found: C, 54.70; H, 4.24; N, 35.10.

PZOAP. Pale yellow powder (mp 258−259 °C). ^{1}H NMR (300 MHz, DMSO-d_6, 25 °C): 10.70 (s, 1H, OH), 9.21 (s, 1H, Ar), 8.89 (d, 1H, Ar), 8.78 (d, 1H, Ar), 8.63 (d, 1H, Ar), 8.20 (d, 1H, Ar), 7.94 (m, 1H, Ar), 7.52 (m, 1H, Ar), 7.11 (s, 2H, NH_2). Mass spectrum (major mass peaks, *m*/*z*): 242 (M), 225, 224 (M − NH_3 and M − H_2O, respectively), 163, 107, 79. IR (Nujol mull, cm^{-1}): 3400, 3306, (νNH_2, νOH); 1664 (s) ($\nu C{=}O$); 1620 (m) ($\nu C{=}N$). Anal. Calcd for $C_{11}H_{10}N_6O$: C, 54.54; H, 4.16; N, 34.69. Found: C, 54.39; H, 4.08; N, 34.88.

6POAP. Pale yellow powder (mp > 300 °C). ^{1}H NMR (300 MHz, DMSO-d_6, 25 °C): 11.50 (br s, 1H, OH) 8.69 (m, 1H, Ar), 8.20 (m, 1H, Ar), 8.00 (m, 1H, Ar), 7.57 (m, 2H, Ar), 6.92 (m, 1H, Ar), 6.53 (m, 1H, Ar), 4.05 (br s, 2H, NH_2). Mass spectrum (major mass peaks, *m*/*z*): 257 (M), 239 (M − H_2O), 223, 183, 163, 107. IR (Nujol mull, cm^{-1}): 3287 (OH, νNH_2) (m); 1688 (s) ($\nu C{=}O$); 1650 (s) ($\nu C{=}N$); 1000 (m) (νpy). Anal. Calcd for $C_{12}H_{11}N_5O_2 \cdot 3H_2O$: C, 46.29; H, 5.46; N, 22.50. Found: C, 46.28; H, 4.90; N, 22.27.

General Procedure for the Synthesis of Complexes 1 − 9. The appropriate diazine ligand (1 mmol) was added to a hot solution of the appropriate metal salt (1 mmol) in 25 mL of aqueous methanol (60:40; H_2O:CH_3OH). The resulting suspension was stirred with heating until complete dissolution of the ligand occurred. The complex solution was allowed to cool to room temperature and filtered. Unless stated otherwise crystals suitable for X-ray diffraction formed from the filtrate after standing for 1−2 weeks. In some cases lattice solvent content differs between the X-ray sample and the analytical sample, due to vacuum-drying of the sample prior to elemental analysis.

[Cu_4(POAP-H)$_4$(H_2O)$_2$](ClO_4)$_4$·4H_2O (1). Green crystals. Yield (80%). IR (Nujol mull, cm^{-1}): 3436 (w) (νH_2O); 3353 (w) (νNH_2); 1666 (s) ($\nu C{=}N$); 1088 (s) (νClO_4^-); 622 (m) (δClO_4^-). Vis (Nujol mull): λ (nm) 653. Vis (H_2O): λ (nm) (ϵ (M^{-1} cm^{-1})) 661 (404). Anal. Calcd for $[Cu_4(C_{12}H_{10}N_5O)_4](ClO_4)_4 \cdot 4H_2O$: C, 34.21; H, 2.87; N, 16.62. Found: C, 34.25; H, 2.49; N, 16.68.

[Cu_4(POAP-H)$_4$(H_2O)$_2$](NO_3)$_4$·4H_2O (2). Green crystals. Yield (74%). IR (Nujol mull, cm^{-1}): 3399 (w) (νH_2O); 3303 (w) (νNH_2); 1748 (w) ($\nu_1 + \nu_4$ NO_3^-); 1669 (s) ($\nu C{=}N$); 1011 (m) (νpy). Vis (Nujol mull): λ (nm) 678. Vis (H_2O): λ (nm) (ϵ (M^{-1} cm^{-1})) 668 (400). Anal. Calcd for $[Cu_4(C_{12}H_{10}N_5O)_4](NO_3)_4 \cdot 4H_2O$: C, 37.55; H, 3.15; N, 21.90. Found: C, 37.55; H, 3.15; N, 22.03.

[Cu_4(POAPZ-H)$_4$(H_2O)](NO_3)$_4$·3H_2O (3). Dark brown crystals. Yield (67%). IR (Nujol mull, cm^{-1}): 3498 (w), 3416 (w) (νH_2O); 3304 (w)(νNH_2); 1748 (w) ($\nu_1 + \nu_4$ NO_3^-); 1666 (s) ($\nu C{=}N$); 1037 (m) (νpy). Vis (Nujol mull): λ (nm) 718. Vis (H_2O): λ (nm) (ϵ (M^{-1} cm^{-1})) 715 (322). Anal. Calcd for $[Cu_4(C_{11}H_9N_6O)_4](NO_3)_4 \cdot 3H_2O$: C, 34.74; H, 2.78; N, 25.78. Found: C, 34.40; H, 2.75; N, 25.80.

[**Cu_4(6POAP-H)$_4$](ClO_4)$_4$ (4).** Green powder. Crystals suitable for crystallographic analysis were grown by slow diffusion of diethyl ether into a solution in DMF:MeOH (1:1). Yield based on green powder (92%). IR (Nujol mull, cm^{-1}): 3435 (w) (νH_2O); 3347 (w) (νNH_2); 1672 (s) ($\nu C{=}N$); 1062 (s) (νClO_4^-); 619 (m) (δClO_4^-). Vis (Nujol mull) λ (nm) 661. Vis (H_2O) λ (nm) (ϵ (M^{-1} cm^{-1})) 664 (453). Anal. Calcd for $[Cu_4(C_{12}H_{10}N_5O_2)_4](ClO_4)_4$: C, 34.38; H, 2.40; N, 16.70. Found: C, 34.40; H, 2.44; N, 16.67.

[Cu_4(PZOAP-H)$_4$](NO_3)$_4$·3H_2O (5). Green crystals. Yield (57%). IR (Nujol mull, cm^{-1}): 3600 (w) (νH_2O); 3400 (w), 3350 (w) (νNH_2); 1668 (s) ($\nu C{=}N$); 1050 (m) (νpy). Vis (Nujol mull): λ (nm) 630 (sh), 685. Anal. Calcd for $[Cu_4(C_{11}H_9N_6O)_4](NO_3)_4 \cdot 3H_2O$: C, 34.78; H, 2.79; N, 25.83. Found: C, 34.53; H, 2.53; N, 25.79.

[Ni_4(POAP-H)$_4$(H_2O)$_4$](NO_3)$_4$·8H_2O (6). Orange/brown crystals. Yield (82%). IR (Nujol mull, cm^{-1}): 3425 (w) (νH_2O); 3319 (w) (νNH_2); 1754 (w) ($\nu_1 + \nu_4$ NO_3^-); 1665 (s) ($\nu C{=}N$); 1025 (m) (νpy). Vis (Nujol mull): λ (nm) 964, 603 (sh). Vis (H_2O): λ (nm) (ϵ (M^{-1} cm^{-1})) 974 (91), 595 (sh) (41). Anal. Calcd for $[Ni_4(C_{12}H_{10}N_5O)_4(H_2O)_4](NO_3)_4 \cdot 8H_2O$: C, 34.73; H, 3.89; N, 20.25. Found: C, 34.42; H, 3.35; N, 20.64.

[Ni_4(POAP-H)$_4$Cl(H_2O)$_3$]Cl_3·10.5H_2O (7). Brown crystals. Yield (62%). IR (Nujol mull, cm^{-1}): 3443−3396 (w) (νH_2O); 3315 (w) (νNH_2); 1686 (s) ($\nu C{=}N$); 1017 (m) (νpy). Vis (Nujol mull): λ (nm) 971, 601 (sh). Vis (H_2O): λ (nm) (ϵ (M^{-1} cm^{-1})) 973 (110), 595 (sh) (36). Anal. Calcd for $[Ni_4(C_{12}H_{10}N_5O)_4Cl(H_2O)_3]Cl_3 \cdot 10.5H_2O$: C, 36.47; H, 4.27; N, 17.72. Found: C, 36.45; H, 3.55; N, 17.76.

[Ni_4(POAPZ-H)$_4$(H_2O)$_4$](ClO_4)$_4$·3H_2O (8). Brown powder. Yield (64%). IR (Nujol mull, cm^{-1}): 3450 (w) (νH_2O); 3347 (w) (νNH_2); 1660 (s) ($\nu C{=}N$); 1092 (s), 622 (m) (δClO_4^-). Vis (Nujol mull): λ (nm) 970, 630. Vis (H_2O): λ (nm) (ϵ (M^{-1} cm^{-1})) 972 (68), 621 (sh) (51). Anal. Calcd for $[Ni_4(C_{11}H_9N_6O)_4(H_2O)_4](ClO_4)_4 \cdot 3H_2O$: C, 30.66; H, 2.92; N, 19.50. Found: C, 30.70; H, 2.72; N, 19.37.

[Ni_4(PZOAP-H)$_4$(H_2O)$_4$](ClO_4)$_4$·5H_2O (9). Brown crystals. Yield (70%). IR: 3445 (m) (νH_2O), 3345 (m) (νNH_2), 1658 ($\nu C{=}N$), 1094 (νClO_4^-). Vis (Nujol mull): λ (nm) 994, 650 (sh). Anal. Calcd for $[Ni_4(C_{11}H_9N_6O)_4(H_2O)_4](ClO_4)_4 \cdot 5H_2O$: C, 30.04; H, 3.07; N, 19.11. Found: C, 30.05; H, 2.94; N, 19.29.

Crystallographic Data Collection and Refinement of the Structures. Data collections for **2**, **5**, **6**, and **9** were made using graphite-monochromated Mo Kα X-radiation with a Siemens SMART CCD detector diffractometer equipped with a Cryostream[33] N_2 flow cooling device. Series of narrow ω-scans (0.3°) were performed at several ϕ-settings in such a way as to cover a hemisphere or a full sphere of data to a maximum resolution of 0.7 Å. Cell parameters were determined and refined within SMART[34] using the centroid values of approximately 500 selected reflections with 2 Θ values between 20 and 45°. Raw frame data were integrated using the SAINT program.[35] The data were corrected for absorption by an empirical ψ-scan based method.[36] The structures were solved using Direct Methods and refined by full-matrix least squares on F^2.[36]

[Cu_4(POAP-H)$_4$(H_2O)$_2$] (NO_3)$_4$·4H_2O (2). A dark green, plate-like crystal with dimensions 0.4 × 0.31 × 0.06 mm was used for the measurements. A total of 21 171 data points were measured which were merged to 6877 unique data with an agreement factor of 0.051. The monoclinic space group *C*2/*c* could not be determined unambiguously

---

(32) Xu, Z.; Thompson, L. K.; Miller, D. O.; Clase, H. J.; Howard, J. A. K.; Goeta, A. E. *Inorg. Chem.* **1998**, *37*, 3620.

(33) Cosier, J.; Glazer, A. M. *J. Appl. Crystallogr.* **1986**, *19*, 105.

(34) Siemens 1996. SMART. Data Collection Software. Ver. 4.050; Siemens Analytical X-ray Instruments Inc., Madison, WI.

(35) Siemens 1996. SAINT. Data Reduction Software. Version 4.050; Siemens Analytical X-ray Instruments Inc., Madison, WI.

(36) Sheldrick, G. M. 1995. SHELXTL 5.04/VMS. An integrated system for solving, refining and displaying crystal structures from diffraction data; Siemens Analytical X-ray Instruments Inc., Madison, WI.

Table 1. Summary of Crystallographic Data for [Cu_4((POAP-H)$_4$(H_2O)$_2$](NO_3)$_4$·4H_2O (**2**), [Cu_4((POAPZ-H)$_4$(H_2O)](NO_3)$_4$·3 H_2O (**3**), [Cu_4(6POAP-H)$_4$](ClO_4)$_4$ (**4**), [Cu_4(PZOAP-H)$_4$](NO_3)$_4$·3H_2O (**5**), [Ni_4(POAP-H)$_4$(H_2O)$_4$](NO_3)$_4$·8H_2O (**6**), and Ni_4(PZOAP-H)$_4$(H_2O)$_4$](ClO_4)$_4$·5H_2O (**9**)

compd	**2**[a]	**3**[b]	**4**[b]	**5**[a]	**6**[a]	**9**[a]
empirical formula	$C_{24}H_{21}N_{22}O_{20.4}Cu_2$	$C_{44}H_{43.3}N_{28}O_{19.65}Cu_4$	$C_{48}H_{48}N_{20}O_{28}Cu_4Cl_4$	$C_{22}H_{27}O_{12.5}N_{14}Cu_4$	$C_{48}H_{53}O_{24.5}N_{23.5}Ni_4$	$C_{44}H_{54}O_{28}N_{24}Cl_4Ni_4$
fw	770.00	1532.89	1749.02	814.66	1585.98	1743.75
space group	*C*2/*c*	*P*2$_1$/*c*	*C*2/*c*(#15)	*P*2$_1$/*n*	$P\bar{1}$	*Pbcn*
a (Å)	20.479(3)	14.12(1)	22.646(4)	14.3573(3)	12.0509(6)	14.368(4)
b (Å)	14.920(2)	14.116(3)	25.842(5)	10.8910(6)	12.7498(6)	25.469(7)
c (Å)	19.671(3)	29.043(4)	12.349(5)	20.536(1)	23.1208(11)	18.479(5)
α (deg)	90	90	90	90	93.105(1)	90
β (deg)	90.591(4)	94.50(3)	110.34(2)	96.975(4)	100.150(1)	90
γ (deg)	90	90	90	90	108.505(1)	90
V (Å^3)	6010(3)	5771(4)	7110(3)	3187.4(3)	3292.9(3)	6762(3)
ρ_{calcd} (g cm^{-3})	1.702	1.764	1.634	1.698	1.600	1.713
Z	8	4	4	4	2	4
μ (mm^{-1})	1.494	1.556	3.555	1.419	1.222	1.355
λ (Å)	0.71073	0.71069	1.54178(Cu Kα)	0.71073	0.71073	0.71073
T (K)	150(2)	299(2)	299	150(2)	193(2)	100(2)
R_1 (*R*)[c]	0.0650	0.049(*R*)	0.080(*R*)	0.0431	0.0871	0.0449
wR_2 (R_w)[c]	0.1365	0.047(R_w)	0.085(R_w)	0.0784	0.1992	0.1043

[a] Siemens Smart data. [b] Rigaku data. [c] $1R_1 = \Sigma||F_o| - |F_c||/\Sigma|F_o|$, $wR_2 = [\Sigma[w(|F_o|^2 - |F_c|^2)^2]/\Sigma[w(|F_o|^2)^2]]^{1/2}$, $R = \Sigma||F_o| - |F_c||/\Sigma|F_o|$, $R_w=[(\Sigma w(|F_o| - |F_c|)^2/\Sigma wF_o^2)]^{1/2}$.

from the systematic absences. However a clearly incorrect result from *Cc* and the satisfactory refinement of the structure in *C*2/*c* confirmed this space group assignment. All non-hydrogen atoms were refined with anisotropic atomic displacement parameters (adps) except those of one nitrate group and one water molecule, which were disordered and modeled as two sites with occupancy factors of 0.8 and 0.2. Hydrogen atoms were placed in geometrically calculated positions and given isotropic adps 1.2 times that of the parent atom, except for the hydrogen atoms of the water molecules which were not located.

Crystal data collection and structure refinement for **5**, **6**, and **9** were carried out in a similar manner. Abbreviated crystal data for **2**, **5**, **6**, and **9** are given in Table 1.

[Cu_4(POAPZ-H)$_4$(H_2O)](NO_3)$_4$·3H_2O (3). The crystals of **3** are brown and irregular in appearance. The diffraction intensities of an approximately 0.35 × 0.20 × 0.40 mm crystal were collected with graphite-monochromated Mo Kα X-radiation using a Rigaku AFC6S diffractometer at 299(1) K and the $\omega-2\Theta$ scan technique to a $2\Theta_{max}$ value of 55.12°. A total of 14 412 reflections were measured, of which 13 864 were considered unique ($R_{int} = 0.026$), and 7932 were considered significant with $I_{net} > 2.0\sigma(I_{net})$. The intensities of three representative reflections, which were measured after every 150 reflections, remained constant throughout the data collection, indicating crystal and electronic stability (no decay correction was applied). An empirical absorption correction, based on azimuthal scans of several reflections, was applied and resulted in transmission factors ranging from 0.79 to 1.00. The data were corrected for Lorentz and polarization effects. The cell parameters were obtained from the least-squares refinement of the setting angles of 24 carefully centered reflections with 2Θ in the range 8.70−29.70°.

The structure was solved by direct methods.[37,38] All atoms except hydrogen were refined anisotropically. Hydrogen atoms were optimized by positional refinement, with isotropic thermal parameters set 20% greater than those of their bonded partners at the time of their inclusion. However they were fixed for the final round of refinement. The final cycle of full-matrix least-squares refinement was based on 7932 observed reflections ($I > 2.00\sigma(I)$) and 874 variable parameters and converged with unweighted and weighted agreement factors of $\Sigma||F_o| - |F_c||/\Sigma|F_o| = 0.049$ and $R_w = [(\Sigma w(|F_o| - |F_c|)^2/\Sigma wF_o^2)]^{1/2} = 0.047$. The maximum and minimum peaks on the final difference Fourier map correspond to 0.56 and −0.56 electrons Å^{-3} respectively. Neutral atom scattering factors[39] and anomalous-dispersion terms[40,41] were taken from the usual sources. All calculations were performed with the teXsan[42] crystallographic software package. Crystal data collection and structure refinement for **4** were carried out in a similar manner. Abbreviated crystal data for **3** and **4** are given in Table 1.

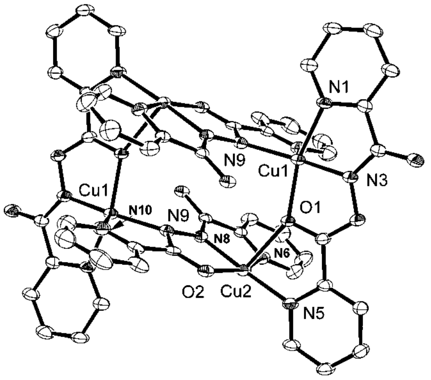

Figure 1. Structural representation of the cation in [Cu_4(POAP-H)$_4$(H_2O)$_2$](NO_3)$_4$·4H_2O (**2**) (40% probability thermal ellipsoids).

Results and Discussion

Structures. [Cu_4(POAP-H)$_4$(H_2O)$_2$](NO_3)$_4$·4H_2O (2). The structure of the cation in **2** is illustrated in Figure 1, and important bond distances and angles are listed in Table 2. The cation consists of a rectangular cluster involving four square-pyramidal copper(II) centers bridged alternately by alkoxide oxygen and diazine N_2 groups. The Cu(1) centers have CuN_4O chromophores, while the Cu(2) atoms have CuN_3O_2 chromophores. Cu(1) and Cu(2) are linked equatorially by nitrogen atoms N(8) and N(9) of the N−N bridge along the long edge of the rectangle, and by O(1) in an axial/equatorial fashion along the short edge of the rectangle (Cu(1)−O(1) 2.035(3) Å, Cu(2)−O(1) 2.325(3) Å). The angle subtended at O(1) is quite large (139.9(2)°), and the torsion angle Cu(1)−N(9)−N(8)−Cu(2) (158.8°) indicates an almost flat arrangement of the short Cu−N (diazine) bonds about the N−N single bond. This arrangement is propagated around the rectangle by two planar

---

(37) Gilmore, C. J. *J. Appl. Crystallogr.* **1984**, *17*, 42.

(38) Beurskens, P. T. DIRDIF: Technical Report 1984/1; Crystallography Laboratory, Toernooiveld, 6525 Ed Nijmegen, Netherlands.

(39) Cromer, D. T.; Waber, J. T. *International Tables for X-ray Crystallography;* The Kynoch Press: Birmingham, U.K., 1974; Vol. IV, Table 2.2A.

(40) Ibers, J. A.; Hamilton, W. C. *Acta Crystallogr.* **1964**, *17,* 781.

(41) Cromer, D. T. *International Tables for X-ray Crystallography;* The Kynoch Press: Birmingham, U.K. 1974; Vol. IV, Table 2.3.1.

(42) teXsan for Windows (version 1.04); Molecular Structure Corp., The Woodlands, TX, 1997−1998.

Table 2. Interatomic Distances (Å) and Angles (deg) Relevant to the Copper Coordination Spheres in **2**

Cu(1)−N(3)	1.900(4)	Cu(2)−N(6)	2.010(4)
Cu(1)−N(9)#1[a]	2.000(4)	Cu(2)−O(2)	2.033(3)
Cu(1)−O(1)	2.035(3)	Cu(2)−O(1)	2.325(3)
Cu(1)−N(1)	2.063(4)	N(8)−N(9)	1.385(5)
Cu(1)−N(10)#1	2.193(4)	Cu(1)−Cu(2)	4.759(1)
Cu(2)−N(8)	1.909(4)	Cu(1)−Cu(2)#1	4.0969(9)
Cu(2)−N(5)	1.968(4)		

N(3)−Cu(1)−N(9)#1	167.6(2)	N(8)−Cu(2)−N(6)	80.6(2)
N(3)−Cu(1)−O(1)	78.8(2)	N(5)−Cu(2)−N(6)	98.7(2)
N(9)#1−Cu(1)−O(1)	98.07(14)	N(8)−Cu(2)−O(2)	79.5(2)
N(3)−Cu(1)−N(1)	79.1(2)	N(5)−Cu(2)−O(2)	101.2(2)
N(9)#1−Cu(1)−N(1)	100.9(2)	N(6)−Cu(2)−O(2)	160.09(14)
O(1)−Cu(1)−N(1)	154.5(2)	N(8)−Cu(2)−O(1)	100.07(13)
N(3)−Cu(1)−N(10)#1	114.7(2)	N(5)−Cu(2)−O(1)	77.34(14)
N(9)#1−Cu(1)−N(10)#1	77.8(2)	N(6)−Cu(2)−O(1)	91.21(14)
O(1)−Cu(1)−N(10)#1	106.29(14)	O(2)−Cu(2)−O(1)	92.98(12)
N(1)−Cu(1)−N(10)#1	94.3(2)	Cu(1)−O(1)−Cu(2)	139.9(2)
N(8)−Cu(2)−N(5)	177.3(2)		

[a] Symmetry transformations used to generate equivalent atoms: #1, $-x + 1/2$, $-y + 1/2$, $-z$.

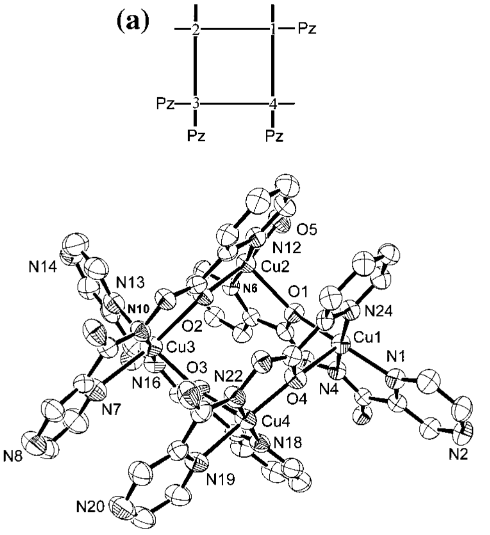

Figure 2. Structural representation of the cation in $[Cu_4(POAPZ-H)_4(H_2O)](NO_3)_4\cdot 3H_2O$ (**3**) (40% probability thermal ellipsoids). (a) Schematic representation of the ligand arrangements in **3** (pz = pyrazine).

Table 3. Interatomic Distances (Å) and Angles (deg) Relevant to the Copper Coordination Spheres in **3**

Cu(1)−O(1)	2.013(3)	Cu(3)−N(10)	1.966(3)
Cu(1)−O(4)	2.254(3)	Cu(3)−N(13)	2.108(4)
Cu(1)−N(1)	2.072(3)	Cu(3)−N(16)	1.913(3)
Cu(1)−N(4)	1.901(3)	Cu(4)−O(3)	2.209(3)
Cu(1)−N(24)	1.979(3)	Cu(4)−O(4)	2.023(3)
Cu(2)−O(1)	2.276(3)	Cu(4)−N(18)	1.968(3)
Cu(2)−O(2)	1.952(3)	Cu(4)−N(19)	2.101(3)
Cu(2)−O(5)	1.995(3)	Cu(4)−N(22)	1.896(3)
Cu(2)−N(6)	1.997(3)	Cu(1)−Cu(2)	4.044(1)
Cu(2)−N(12)	1.997(3)	Cu(1)−Cu(4)	4.017(1)
Cu(3)−O(2)	2.371(3)	Cu(2)−Cu(3)	4.076(1)
Cu(3)−O(3)	2.055(3)	Cu(3)−Cu(4)	4.016(1)
Cu(3)−N(7)	2.349(4)		

O(1)−Cu(1)−O(4)	91.87(9)	O(3)−Cu(4)−N(22)	105.7(1)
O(3)−Cu(3)−N(10)	103.8(1)	O(1)−Cu(2)−N(12)	106.8(1)
O(1)−Cu(1)−N(1)	155.7(1)	O(4)−Cu(4)−N(18)	99.5(1)
O(3)−Cu(3)−N(13)	154.7(1)	O(2)−Cu(2)−O(5)	167.6(1)
O(1)−Cu(1)−N(4)	79.2(1)	O(4)−Cu(4)−N(19)	155.2(1)
O(3)−Cu(3)−N(16)	78.6(1)	O(2)−Cu(2)−N(6)	93.1(1)
O(1)−Cu(1)−N(24)	101.2(1)	O(4)−Cu(4)−N(22)	79.1(1)
N(7)−Cu(3)−N(10)	74.9(1)	O(2)−Cu(2)−N(12)	82.9(1)
O(4)−Cu(1)−N(1)	105.1(1)	N(18)−Cu(4)−N(19)	101.8(1)
N(7)−Cu(3)−N(13)	95.5(1)	O(5)−Cu(2)−N(6)	88.8(1)
O(4)−Cu(1)−N(4)	107.4(1)	N(18)−Cu(4)−N(22)	175.3(1)
N(7)−Cu(3)−N(16)	98.9(1)	O(5)−Cu(2)−N(12)	94.2(1)
O(4)−Cu(1)−N(24)	78.9(1)	N(19)−Cu(4)−N(22)	78.7(1)
N(10)−Cu(3)−N(13)	100.4(1)	N(6)−Cu(2)−N(12)	174.3(1)
N(1)−Cu(1)−N(4)	79.1(1)	Cu(1)−O(1)−Cu(2)	141.0(1)
N(10)−Cu(3)−N(16)	173.6(1)	O(2)−Cu(3)−O(3)	87.5(1)
N(1)−Cu(1)−N(24)	99.1(1)	O(2)−Cu(3)−N(7)	148.2(1)
N(13)−Cu(3)−N(16)	78.1(1)	O(2)−Cu(3)−N(10)	73.3(1)
N(4)−Cu(1)−N(24)	173.8(1)	Cu(2)−O(2)−Cu(3)	140.9(1)
O(3)−Cu(4)−O(4)	108.5(1)	O(2)−Cu(3)−N(13)	92.6(1)
O(1)−Cu(2)−O(2)	99.4(1)	O(2)−Cu(3)−N(16)	112.9(1)
O(3)−Cu(4)−N(18)	79.0(1)	O(3)−Cu(3)−N(7)	97.7(1)
O(1)−Cu(2)−O(5)	93.0(1)	Cu(3)−O(3)−Cu(4)	140.7(1)
O(3)−Cu(4)−N(19)	88.0(1)	Cu(1)−O(4)−Cu(4)	139.8(1)
O(1)−Cu(2)−N(6)	77.8(1)		

tetradentate ligands, which are bound to each adjacent pair of metals by five bonds, two from the oxygen, two from the pyridines and one from the diazine nitrogen, and two pentadentate ligands which are bound by both diazine and pyridine nitrogen sites, and by a terminal alkoxide site. N(1), N(3), and N(5) are bonded to equatorial metal sites, while O(1) is bonded to the equatorial site of Cu(1) and the axial site of Cu(2). This leads to a large separation of 4.759(1) Å between Cu(1) and Cu(2) linked by the diazine, and a shorter (4.0969(9) Å) separation between Cu(1) and Cu(2) linked by the oxygen.

$[Cu_4(POAPZ-H)_4(H_2O)](NO_3)_4\cdot 3H_2O$ (3). The structure of the cation in **3** is illustrated in Figure 2, and bond distances and angles are listed in Table 3. The cationic cluster fragment consists of a square arrangement of copper(II) centers bridged just by alkoxide oxygen atoms. Two oxygens (O(1) and O(3)) are located below the Cu_4 plane, and two (O(2) and O(4)) are located above the plane in a boatlike arrangement. Cu(1) and Cu(4) are square-pyramidal with CuN_3O_2 chromophores, and long axial contacts to the bridging oxygens (Cu(1)−O(4) 2.254(3) Å, Cu(4)−O(3) 2.209(3) Å). Cu(3) has an axially distorted tetragonal structure, with a CuN_4O_2 chromophore, and long contacts to O(2) and N(7) (Cu(3)−O(2) 2.371(3) Å, Cu(3)−N(7) 2.349(4) Å). Cu(2) nominally has a square-pyramidal structure with a long axial contact to O(1) (Cu(2)−O(1) 2.276(3) Å), but another contact to nitrate oxygen O(6) (Cu(2)−O(6) 2.644(3) Å) suggests that Cu(2) probably should be considered to be six-coordinate as well. This contact is stabilized by a hydrogen bond between nitrate oxygen O(7) and bonded water O(5) (O(5)−O(7) 2.701(4) Å; O(5)−H(5OA)−O(7) 160.9°).

The Cu_4 square is unsymmetric, with four unequal axial contacts from the copper to the oxygen bridges. This leads to somewhat different Cu−Cu separations (Cu(1)−Cu(2) 4.044(1) Å, Cu(1)−Cu(4) 4.017(1) Å, Cu(3)−Cu(4) 4.016(1) Å, Cu(2)−Cu(3) 4.076(1) Å), but the oxygen bridge angles are similar, in the range 139.8−141.0° The POAPZ ligands allow an orientational distinction to be made between the four ligands. The ligands are arranged in parallel pairs around the tetra-copper square, with two pyrazine ends bonded to Cu(3), one to Cu(4) and one to Cu(1). This produces an unsymmetrical arrangement of the four ligands around the square (Figure 2a).

$[Cu_4(6POAP-H)_4](ClO_4)_4$ (4). The structure of the tetranuclear cluster cation is illustrated in Figure 3, and important bond distances and angles are listed in Table 4. The four square-pyramidal copper centers are arranged symmetrically in a square, with the two pairs of parallel ligands arranged above and below the Cu_4 plane. The 2-fold rotational symmetry leads to two equivalent pairs of copper centers (Figure 4), with an alternating arrangement of axial (Cu(1)−O(1) 2.248(6) Å, Cu(2)−O(3) 2.223(6) Å) and equatorial Cu−O bonds (Cu(1)−O(3) 2.003(6) Å, Cu(2)−O(1) 2.000(6) Å) around the square. Again the

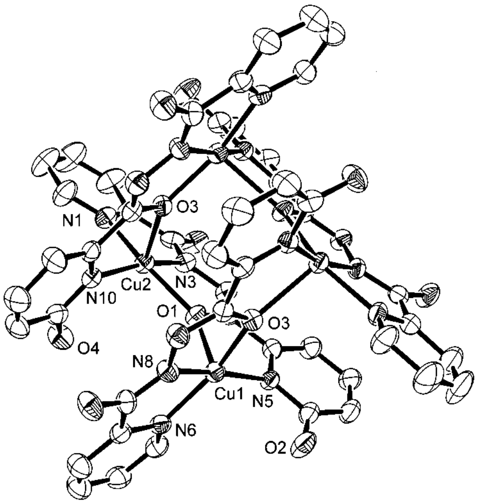

Figure 3. Structural representation of the cation in [Cu_4(6POAP-H)$_4$]-(ClO_4)$_4$ (**4**) (40% probability thermal ellipsoids).

Table 4. Interatomic Distances (Å) and Angles (deg) Relevant to the Copper Coordination Spheres in **4**

Cu(1)−O(1)	2.248(6)	Cu(2)−O(3)	2.223(6)
Cu(1)−O(3)	2.003(6)	Cu(2)−N(1)	2.037(8)
Cu(1)−N(5)	1.962(7)	Cu(2)−N(3)	1.908(7)
Cu(1)−N(6)	2.050(8)	Cu(2)−N(10)	1.990(8)
Cu(1)−N(8)	1.900(8)	Cu(1)−Cu(2)	3.987(3)
Cu(2)−O(1)	2.000(6)	Cu(1)′−Cu(2)	3.958(3)
O(1)−Cu(1)−O(3)	95.0(3)	O(1)−Cu(2)−N(1)	157.5(3)
O(1)−Cu(1)−N(5)	77.0(3)	O(1)−Cu(2)−N(3)	78.9(3)
O(1)−Cu(1)−N(6)	94.4(3)	O(1)−Cu(2)−N(10)	99.3(3)
O(1)−Cu(1)−N(8)	113.6(3)	O(3)−Cu(2)−N(1)	96.1(3)
O(3)−Cu(1)−N(5)	97.4(3)	O(3)−Cu(2)−N(3)	115.8(3)
O(3)−Cu(1)−N(6)	158.4(3)	O(3)−Cu(2)−N(10)	77.1(3)
O(3)−Cu(1)−N(8)	79.0(3)	N(1)−Cu(2)−N(3)	79.4(3)
N(5)−Cu(1)−N(6)	103.6(3)	N(1)−Cu(2)−N(10)	100.5(3)
N(5)−Cu(1)−N(8)	168.9(3)	N(3)−Cu(2)−N(10)	167.1(4)
N(6)−Cu(1)−N(8)	79.5(3)	Cu(1)−O(1)−Cu(2)	139.6(3)
O(1)−Cu(2)−O(3)	98.5(3)	Cu(1)−O(3)−Cu(2)	138.9(3)

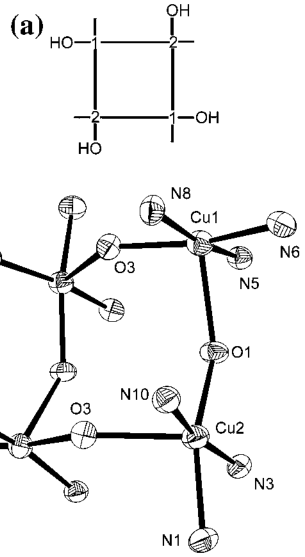

Figure 4. Structural representation of the tetranuclear core in **4**. (a) Schematic representation of the ligand arrangements in **4**.

oxygen bridges are arranged in pairs above and below the Cu_4 plane in a boatlike conformation. The Cu−Cu separations are close to 4 Å (Cu(2)−Cu(1) 3.987(3) Å, Cu(1)′−Cu(2) 3.958(3) Å), with oxygen bridge angles of 139.6(3)° and 138.9(3)° at O(1) and O(3), respectively.

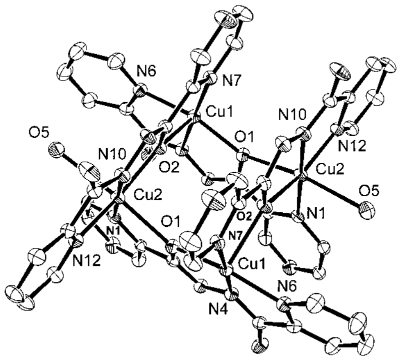

Figure 5. Structural representation of the cation in [Cu_4(PZOAP-H)$_4$]-(NO_3)$_4$·3H_2O (**5**) (40% probability thermal ellipsoids).

The unsymmetrical ligand 6-POAP is different from POAPZ in that the non-pyridine group is attached to the OH end of the ligand. The four 6-hydroxy pyridine ends are arranged at the corners of the square in a rotationally symmetric fashion (Figures 3, 4a), such that oxygens O(2) and O(4) are positioned to create a steric blocking effect to possible incoming sixth ligands (Cu(1)−O(2) 2.941(3) Å, Cu(2)−O(4) 2.969(3) Å).

[Cu_4(PZOAP-H)$_4$](NO_3)$_4$·3H_2O (5). The structure of the tetranuclear cationic cluster is illustrated in Figure 5, and important bond distances and angles are listed in Table 5. The four ligands are arranged in two parallel pairs, above and below the tetracopper square, with the familiar alkoxide bridging arrangement. Copper−copper separations are close to 4 Å (Cu(1)−Cu(2)′ 4.0457(4) Å, Cu(1)−Cu(2) 4.0575(4) Å), with alkoxide bridge angle close to 140° (Cu(1)−O(1)−Cu(2) 140.58(7)°, Cu(1)−O(2)−Cu(2)′ 140.55(7)°). The Cu(1) centers are square-pyramidal, but a long significant contact between Cu(2) and O(5) (2.461(2) Å) indicates that the Cu(2) centers are six-coordinate. The ligands are oriented in the same way as in **4**, with the pyrazine ends bonded individually to each copper center.

The copper−oxygen bonds within the ring alternate with long and short contacts (Cu(1)−O(1) 2.015(1) Å, Cu(2)−O(1) 2.294(2) Å, Cu(2)−O(2) 2.0362(2) Å, Cu(1)−O(2) 2.261(1) Å), such that the coppers are linked alternately by the oxygen bridges with axial and equatorial contacts.

[Ni_4(POAP-H)$_4$(H_2O)$_4$](NO_3)$_4$·8H_2O (6). The structure of the tetranuclear cluster cation is illustrated in Figure 6, and important bond distances and angles are listed in Table 6. A view of the tetranuclear core with just the immediate donor atoms is shown in Figure 7. The four pseudo-octahedral nickel(II) centers are arranged in a slightly distorted square (displacement of the metals from the M_4 least-squares plane; Ni(1) −0.144 Å, Ni(2) 0.145 Å, Ni(3) −0.145 Å, Ni(4) 0.144 Å), and are bridged by four alkoxide oxygens from the four deprotonated ligands, arranged in pairs above and below the Ni_4 plane in a boatlike conformation. O−Ni−O angles fall in the range 89.6−94.7° and the metal−metal separations fall in the range 3.95−3.98 Å. The ligands are arranged in two groups of parallel pairs, with each ligand in a roughly eclipsed arrangement compared with its partner. The total coordination requirement of the four metals (24 bonds) is completed by four ligands, which fill 20 coordination sites, and four water molecules, one binding to Ni(2), two to Ni(3), and one to Ni(4). This leads to a unique situation involving three different nickel(II) centers, with *cis*-NiN_4O_2 (C; Ni(1)), *mer*-NiN_3O_3 (M; Ni(2), Ni(4)), and *trans*-NiN_2O_4 (T; Ni(3)) chromophores. The arrangement of the nickel centers is illustrated in Figure 7a,

Table 5. Interatomic Distances (Å) and Angles (deg) Relevant to the Copper Coordination Spheres in **5**

Cu(1)−N(4)	1.9080(17)	Cu(2)−O(2)#1[a]	2.0363(15)
Cu(1)−O(1)	2.0153(15)	Cu(2)−N(12)#1	2.0538(18)
Cu(1)−N(7)	2.0194(17)	O(2)−Cu(2)#1	2.0363(15)
Cu(1)−N(6)	2.0618(18)	N(10)−Cu(2)#1	1.9146(17)
Cu(1)−O(2)	2.2608(14)	N(12)−Cu(2)#1	2.0538(18)
O(1)−Cu(2)	2.2936(15)	Cu(1)−Cu(2)#1	4.0457(4)
N(1)−Cu(2)	2.0181(17)	Cu(1)−Cu(2)	4.0575(4)
N(4)−Cu(1)−O(1)	79.16(7)	N(10)#1−Cu(2)−N(1)	178.23(8)
N(4)−Cu(1)−N(7)	177.57(8)	N(10)#1−Cu(2)−O(2)#1	78.67(7)
O(1)−Cu(1)−N(7)	99.86(7)	N(1)−Cu(2)−O(2)#1	99.65(6)
N(4)−Cu(1)−N(6)	79.48(7)	N(10)#1−Cu(2)−N(12)#1	79.59(7)
O(1)−Cu(1)−N(6)	158.62(7)	N(1)−Cu(2)−N(12)#1	102.07(7)
N(7)−Cu(1)−N(6)	101.45(7)	O(2)#1−Cu(2)−N(12)#1	158.26(6)
N(4)−Cu(1)−O(2)	104.46(7)	N(10)#1−Cu(2)−O(1)	103.28(7)
O(1)−Cu(1)−O(2)	96.21(6)	N(1)−Cu(2)−O(1)	77.30(6)
N(7)−Cu(1)−O(2)	77.82(6)	O(2)#1−Cu(2)−O(1)	92.64(6)
N(6)−Cu(1)−O(2)	89.95(7)	N(12)#1−Cu(2)−O(1)	93.01(6)
Cu(1)−O(1)−Cu(2)	140.58(7)	Cu(2)#1−O(2)−Cu(1)	140.55(7)

[a] Symmetry transformations used to generate equivalent atoms: #1 $-x+{}^{1}/_{2}$, y, $-z+{}^{1}/_{2}$.

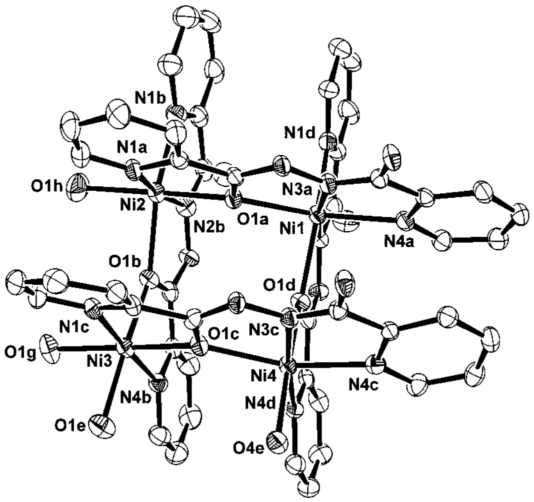

Figure 6. Structural representation of the cation in $[Ni_4(POAP\text{-}H)_4(H_2O)_4](NO_3)_4\cdot 8H_2O$ (**6**) (40% probability thermal ellipsoids).

Table 6. Interatomic Distances (Å) and Angles (deg) Relevant to the Nickel Coordination Spheres in **6**

Ni(1)−N(3A)	1.972(5)	Ni(3)−O(1C)	2.061(4)
Ni(1)−N(2D)	1.979(5)	Ni(3)−O(1E)	2.072(6)
Ni(1)−N(2D)	2.132(5)	Ni(3)−O(1B)	2.096(4)
Ni(1)−N(4A)	2.156(5)	Ni(3)−O(1G)	2.097(6)
Ni(1)−O(1A)	2.176(4)	Ni(4)−N(3C)	1.966(5)
Ni(1)−O(1D)	2.177(4)	Ni(4)−N(4D)	2.053(5)
Ni(2)−N(2B)	1.966(5)	Ni(4)−O(1D)	2.091(4)
Ni(2)−N(1A)	2.044(5)	Ni(4)−O(4E)	2.107(5)
Ni(2)−O(1A)	2.075(4)	Ni(4)−N(4C)	2.107(5)
Ni(2)−O(1H)	2.080(6)	Ni(4)−O(1C)	2.158(4)
Ni(2)−N(1B)	2.115(6)	Ni(1)−Ni(2)	3.969(2)
Ni(2)−O(1B)	2.165(4)	Ni(2)−Ni(3)	3.954(2)
Ni(3)−N(1C)	2.053(5)	Ni(3)−Ni(4)	3.966(2)
Ni(3)−N(4B)	2.059(6)	Ni(4)−Ni(1)	3.977(2)
O(1A)−Ni(1)−O(1D)	89.6(2)	Ni(3)−O(1B)−Ni(2)	136.2(2)
O(1A)−Ni(2)−O(1B)	92.7(2)	Ni(3)−O(1C)−Ni(4)	140.1(2)
O(1C)−Ni(3)−O(1B)	91.7(2)	Ni(4)−O(1D)−Ni(1)	137.5(2)
O(1D)−Ni(4)−O(1C)	94.7(2)	Ni(2)−O(1A)−Ni(1)	138.0(2)

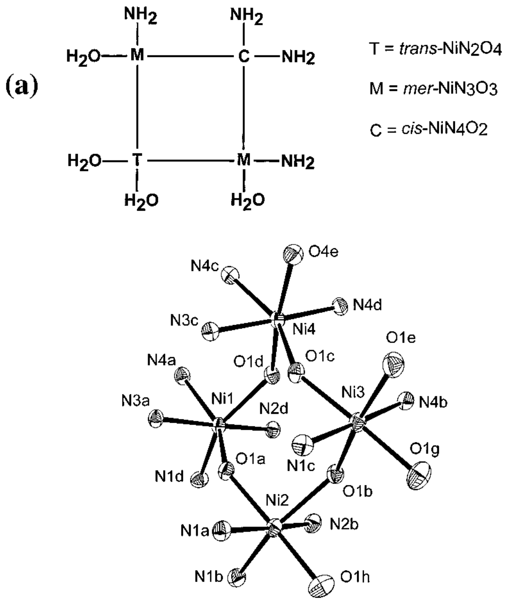

Figure 7. Structural representation of the tetranuclear core in **6**. (a) Schematic representation of the nickel centers and the ligand arrangements in **6**.

which shows the asymmetric disposition of the ligands and the opposite location of the two mer centers.

Nickel−oxygen (alkoxide) bond distances are quite variable, but an interesting trend is observed based on the nickel chromophore. Ni(1) has two long contacts to O(1A) and O(1D) (2.176(4), 2.177(4) Å respectively), Ni(2) and Ni(4) have long and short contacts to O(1B), O(1A) and O(1C), O(1D), respectively (Ni(2)−O(1B) 2.165(4) Å, Ni(2)−O(1A) 2.075(4) Å, Ni(4)−O(1C) 2.158(4) Å, Ni(4)−O(1D) 2.091(4) Å), and Ni(3) has short contacts to O(1B) and O(1C) (2.096(4), 2.061(4) Å respectively). This establishes an asymmetric, alternating *long−short* bridging arrangement within the Ni_4 square. Ni−O−Ni angles fall in the range 136.2−140.1°.

$[Ni_4(POAP\text{-}H)_4Cl(H_2O)_3]Cl_3\cdot 10.5H_2O$ (7). A preliminary structural determination for **7**[43] reveals a similar square cluster to that observed in **6**, and the same equivalent conformation, with the exception that one water molecule is replaced by a coordinated chlorine ligand to give a pseudo-meridional NiN_3O_2Cl structure at the equivalent Ni(4) site. Ni−Ni separations fall in the range 3.91−4.03 Å, and the Ni−O−Ni angles fall in the range 132.8−138.3° for this complex.

$[Ni_4(PZOAP\text{-}H)_4(H_2O)_4](ClO_4)_4\cdot 5H_2O$ (9). The structural representation of the tetranuclear cation is illustrated in Figure 8, and important bond distances and angles are listed in Table

---

[43] Burke, D. M.; Xu, Z.; Parsons, S. R.; Thompson, L. K.; C. Wilson; Howard, J. A. K. Unpublished results.

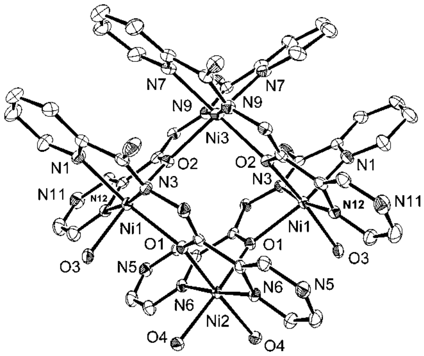

Figure 8. Structural representation of the cation in [Ni_4(PZOAP-H)$_4$(H_2O)$_4$](ClO_4)$_4$·5H_2O (**9**) (50% probability thermal ellipsoids).

Table 7. Interatomic Distances (Å) and Angles (deg) Relevant to the Nickel Coordination Spheres in **9**

Ni(1)−O(1)	2.162(2)	Ni(2)−N(6)	2.038(3)
Ni(1)−O(2)	2.077(2)	Ni(3)−O(2)	2.169(2)
Ni(1)−O(3)	2.055(2)	Ni(3)−N(7)	2.114(3)
Ni(1)−N(1)	2.127(3)	Ni(3)−N(9)	1.970(3)
Ni(1)−N(3)	1.966(3)	N(3)−N(4)	1.400(3)
Ni(1)−N(12)	2.069(3)	Ni(1)−Ni(3)	3.969(2)
Ni(2)−O(1)	2.072(2)	Ni(1)−Ni(2)	3.967(2)
Ni(2)−O(4)	2.083(2)		

O(1)−Ni(1)−O(2)	91.12(8)	O(2c)−Ni(3)−N(9)	109.42(9)
O(1c)−Ni(2)−N(6c)	80.73(9)	N(1)−Ni(1)−N(3)	77.74(10)
O(1)−Ni(1)−O(3)	85.44(8)	N(7c)−Ni(3)−N(9)	97.50(11)
O(4c)−Ni(2)−N(6c)	91.57(9)	N(1)−Ni(1)−N(12)	95.10(10)
O(1)−Ni(1)−N(1)	153.78(9)	N(9)−Ni(3)−N(9c)	172.47(11)
O(2)−Ni(3)−N(7)	153.00(9)	N(3)−Ni(1)−N(12)	171.97(10)
O(1)−Ni(1)−N(3)	76.34(9)	O(2c)−Ni(3)−N(7c)	153.00(9)
O(2)−Ni(3)−N(9)	75.91(9)	O(1)−Ni(2)−O(4)	91.33(8)
O(1)−Ni(1)−N(12)	111.01(9)	O(2c)−Ni(3)−N(9c)	75.91(9)
O(2)−Ni(3)−O(2c)	94.82(8)	O(1)−Ni(2)−N(6)	80.73(9)
O(2)−Ni(1)−O(3)	167.05(9)	N(7)−Ni(3)−N(9)	77.52(10)
O(2)−Ni(3)−N(7c)	89.50(9)	O(1)−Ni(2)−O(1c)	90.48(8)
O(2)−Ni(1)−N(1)	95.99(9)	O(1)−Ni(2)−O(4c)	172.19(8)
O(2)−Ni(3)−N(9c)	109.42(9)	O(1)−Ni(2)−N(6c)	96.22(9)
O(2)−Ni(1)−N(3)	97.20(9)	O(4)−Ni(2)−N(6)	91.57(9)
O(2)−Ni(1)−N(12)	79.77(9)	O(1c)−Ni(2)−O(4)	172.19(8)
O(2c)−Ni(3)−N(7)	89.50(9)	O(4)−Ni(2)−O(4c)	87.89(8)
O(3)−Ni(1)−N(1)	92.54(10)	O(1c)−Ni(2)−N(6)	96.22(9)
N(7)−Ni(3)−N(7c)	98.63(10)	O(4c)−Ni(2)−N(6)	91.52(9)
O(3)−Ni(1)−N(3)	94.12(10)	N(6)−Ni(2)−N(6c)	175.70(11)
N(7)−Ni(3)−N(9c)	97.50(10)	O(1c)−Ni(2)−O(4c)	91.33(8)
O(3)−Ni(1)−N(12)	89.80(10)	Ni(1)−O(1)−Ni(2)	139.08(10)
N(7c)−Ni(3)−N(9c)	77.52(10)	Ni(1)−O(2)−Ni(3)	138.37(10)

7. The square cluster has the same equivalent ligand conformation to **6**, with the same metal ion chromophores, and with the pyrazine ends of the ligands bonded to the nickel centers having the coordinated water molecules. This asymmetric ligand arrangement contrasts with that in **5** where the PZOAP ligands are arranged in a spiral fashion about the cluster. Nickel−nickel separations (Ni(1)−Ni(2) 3.967(2) Å, Ni(1)−Ni(3) 3.969(2) Å) and Ni−O−Ni angles (Ni(1)−O(1)−Ni(2) 139.08(10)°, Ni(1)−O(2)−Ni(3) 138.37(10)°) are comparable with those in **6** and **7**.

Self-Assembly and Structure. The backbone structure of the ligands contains two diazine nitrogens linking two peripheral heterocyclic rings. The ligands are made by the same general strategy in which a hydrazide is reacted with a methyl iminoester. This leads to ligands with pyridine or pyrazine fragments at the ends. The N−N fragment was found to bridge two copper(II), nickel(II), cobalt(III), iron(II), iron(III), and manganese(II) centers in dinuclear complexes with the ligand PAHAP (POAP; OH═NH_2),[30−32] but on changing the NH_2 group to OH a dramatic change in the coordinating ability of the ligand takes place. The OH group deprotonates and acts as a bridge between two adjacent metal ions with three other nitrogens (heterocyclic rings and one diazine) acting as donors, with each ligand behaving in a tetradentate fashion. The NH_2 groups are not involved in coordination. The ligand donor set combination provides a template for binding the two adjacent metals, and then the cluster builds by a self-assembly process, and at the same time attempts to satisfy the coordination requirements of all of the metals. The outcome varies depending on the ligand and the anion, and examples of both homo-metallic and hetero-metallic tetranuclear[43] and homo-metallic pentanuclear (Mn_5)[44] clusters have been found. The most common arrangement so far is a grid of four metals arranged in a distorted square shape, which forms from the assembly of the metals and two pairs of roughly parallel ligands (Figures 2−9). The assembly mechanism is difficult to predict, but one could envisage an initial step of coordination of the ligand at three sites, one pyridine or pyrazine nitrogen, one diazine nitrogen, and the adjacent deprotonated OH, in a meridional fashion, with solvent molecules occupying the other coordination sites. This would be consistent with the reaction stoichiometry. The assembly process could then involve docking of a second metal with a similar coordination environment. The linkage to the second metal would reasonably involve displacement of two cis-coordinated solvent molecules, which would orient the second metal at ∼90°. This process could then continue to complete the square cluster with two ligands above and below the metallic plane. This is illustrated schematically in Figure 9a, leading to a rotationally staggered arrangement of the ligands (arrows point to the NH_2 ends), and possibly one solvent molecule coordinated to each metal in the square metallic plane.

This does occur for **4** and **5**, but for the other square compounds different arrangements exist. For **6**, **7**, and **9** an asymmetric arrangement is found with each parallel pair of ligands pointing in the same direction (Figure 9b), while for **3** one ligand pair points in the same direction, while for the other pair the ligands are opposed (Figure 9c). Clearly more subtle self-assembly effects are at play in these cases, and it is difficult to completely rationalize the assembly processes. An examination of interligand separations reveals no short contacts, e.g., hydrogen bonding between the NH_2 groups. As further structural examples emerge, with these and other related ligands, further insights into the assembly process may be obtained.

Complex **2** has a completely different structure, with a rectangle of copper centers, and an alternating bridging arrangement of alkoxide and diazine groups. This is a rare structural form within this class of compounds, and has only been observed in two other cases, one involving a symmetric hetero-tetranuclear rectangle of two Co(II) and two Fe(II) centers, and the other a homo-tetranuclear Co(II) complex with the ligand POAP.[43] In these cases a pair of tetradentate, and a pair of pentadentate ligands are involved.

Magnetic Properties. Magnetic moments at room temperature for **1**, **3**−**5** are higher than normal values for uncoupled copper(II) complexes ($\mu = 1.88-2.01\ \mu_B$, and suggest either the absence of exchange or the possible presence of ferromagnetic exchange. **2** has a room temperature moment less than the spin-only value, and suggests the presence of antiferromagnetic exchange. Compounds **6**−**9** have room-temperature moments which are typical for Ni(II) complexes with weak antiferromagnetic exchange. Variable temperature magnetic

---

(44) Matthews, C. J.; Xu, Z.; Mandal, S. K.; Thompson, L. K.; Biradha, K.; Poirier, K.; Zaworotko, M. J. *J. Chem. Soc., Chem. Commun.* **1999**, 347.

Table 8. Magnetic Data

compd	$\mu(RT)$ (μ_B)	g	J (cm^{-1})	ρ	TIP (10^6 emu)	θ	10^2R
$[Cu_4(POAP\text{-}H)_4(H_2O)_2](ClO_4)_4\cdot 4H_2O$ (**1**)	1.88	2.124(2)	7.3(1)	0.0004	220	−3.4	0.16
$[Cu_4(POAP\text{-}H)_4(H_2O)_2](NO_3)_4\cdot 4H_2O$ (**2**)	1.68	2.18(1)	−168(1)	0.029(1)	240	0	0.29
$[Cu_4(POAPZ\text{-}H)_4(H_2O)](NO_3)_4\cdot 3H_2O$ (**3**)	1.91	2.119(7)	9.8(4)	0.00002	234	−0.5	0.48
$[Cu_4(6POAP\text{-}H)_4](ClO_4)_4$ (**4**)	1.96	2.060(7)	9.4(4)	0.00004	232	−0.4	0.2
$[Cu_4(PZOAP\text{-}H)_4](NO_3)_4\cdot 3H_2O$ (**5**)	2.01	2.221(5)	8.2(4)	0.0004	242	−0.4	1.1
$[Ni_4(POAP\text{-}H)_4(H_2O)_4](NO_3)_4\cdot 8H_2O$ (**6**)	3.21	2.29(1)	−13.6(2)	0.012	800	0	0.7
$[Ni_4(POAP\text{-}H)_4Cl(H_2O)_3]Cl_3\cdot 10.5H_2O$ (**7**)	3.10	2.18(1)	−10.4(2)	0.014	800	0	0.9
$[Ni_4(POAPZ\text{-}H)_4(H_2O)_4](ClO_4)_4\cdot 3H_2O$ (**8**)	3.27	2.28(1)	−15.9(3)	0.0292	800	0	1.5
$[Ni_4(PZOAP\text{-}H)_4(H_2O)_4](ClO_4)_4\cdot 5H_2O$ (**9**)	3.14	2.205(4)	−13.2(2)	0.005	800	0	0.35

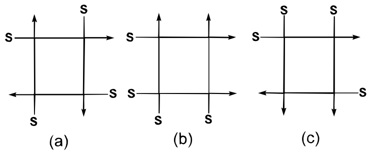

Figure 9. Schematic representation of the various tetranuclear coordination arrangements (S = coordinated solvent, the arrow head points to the NH_2 end of the ligand).

susceptibility data were obtained in the range 4−300 K for all the complexes, and in some cases magnetization versus field measurements were carried out.

3 shows an increase in susceptibility (χ_M) as temperature is decreased, and a plot of μ (per mole) (Figure 10) shows that μ is virtually constant at ~3.8 μ_B down to 100 K and then increases steadily to a value of 4.83 μ_B at 5 K. This behavior is typical of a cluster exhibiting intramolecular ferromagnetic coupling. A magnetization study at 5 K in the range 0−5 T shows marked curvature in the M/H profile extrapolating to saturation at about 6 T. The calculated value of μ of 3.85 μ_B at 5 T is close to the value expected for four copper(II) centers. The variable temperature magnetic data were fitted to an exchange expression (eqs 2, 3) derived from the appropriate isotropic exchange Hamiltonian (eq 1) for a square arrangement of four $S = {}^1/_2$ metal centers (χ_M is the molar susceptibility, ρ is the fraction of paramagnetic impurity, TIP is the temperature independent paramagnetism, θ is a Weiss-like temperature correction; all other terms have their usual significance).

$$H = -2J(S_1\cdot S_2 + S_2\cdot S_3 + S_3\cdot S_4 + S_1\cdot S_4) \tag{1}$$

$$\chi_{M'} = \frac{N\beta^2g^2}{3k(T-\theta)}\,\frac{\Sigma_{S_T}(S_T+1)(2S_T+1)e^{-E(S_T)/kT}}{\Sigma_{S_T}(2S_T+1)e^{-E(S_T)/kT}} \tag{2}$$

$$\chi_M = \chi_{M'}(1-\rho) + \frac{2N\beta^2g^2\rho}{3kT} + \text{TIP} \tag{3}$$

For simplicity the model assumes that all exchange integrals between adjacent pairs of Cu(II) centers are the same. The solid line in Figure 10 represents the best fit of the data to eq 3 and was calculated for $g = 2.119(7)$, $J = 9.8(4)$ cm^{-1}, $\rho = 0.00002$, $\theta = -0.5$ K, TIP = 234 × 10^{-6} emu (per mole), $10^2R = 0.48$ ($R = [\Sigma(\chi_{obs} - \chi_{calc})^2/\Sigma\chi^2_{obs}]^{1/2}$). The positive J value confirms the intramolecular ferromagnetic coupling. The structure shows that all the copper(II) centers are linked by axial/equatorial (orthogonal) contacts through the alkoxide bridges. This would nominally indicate a lack of antiferromagnetic coupling, as observed, but the dominant ferromagnetism is somewhat surprising, and can be attributed to the close proximity of the four copper centers within the square arrangement.

1 shows an increase in χ_M as temperature is decreased, and a plot of μ (per mole) (Figure 11) shows that μ decreases slightly on cooling from a value of 3.76 μ_B at 300 K to 3.73 μ_B at ~150 K and then rises sharply to 3.87 μ_B at 9 K, followed by a decrease at lower temperatures. Above 9 K this is typical of ferromagnetic behavior. A magnetization study at 4.5 K in the range 0−5 T shows marked curvature in the M/H profile extrapolating to saturation at about 7 T. The calculated value of 3.54 μ_B at 5 T approaches the value expected for four copper(II) centers. The decrease in μ from 9 K down to 5 K (Figure 11) indicates the presence of an antiferromagnetic component as well, which may be intermolecular in nature. The data were fitted to eq 3, and the best fit line (Figure 11) was calculated for $g = 2.124(2)$, $J = 7.28(9)$, $\rho = 0.0005$, TIP = 220 × 10^{-6} emu (per mole), $\theta = -3.4$ K, $10^2R = 0.16$. Although a publishable structure for **1** is not available, a preliminary structural determination indicated a square cluster similar to **3**, with four alkoxide bridges, in agreement with the magnetic data.

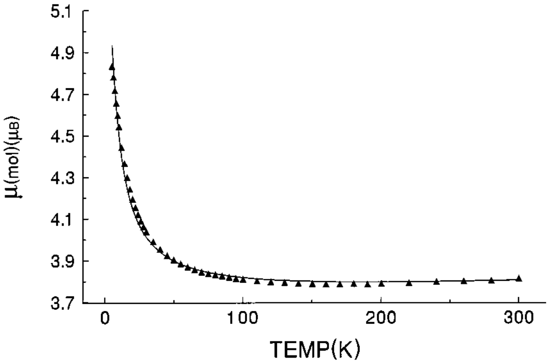

Figure 10. Variable temperature magnetic data for $[Cu_4(POAPZ\text{-}H)_4(H_2O)](NO_3)_4\cdot 3H_2O$ (**3**). The solid line was calculated from eq 3 with $g = 2.119(7)$, $J = 9.8(4)$ cm^{-1}, $\rho = 0.00002$, $\theta = -0.5$ K, TIP = 234 × 10^{-6} emu (per mole), $10^2R = 0.48$ ($R = [\Sigma(\chi_{obs} - \chi_{calc})^2/\Sigma\chi^2_{obs}]^{1/2}$).

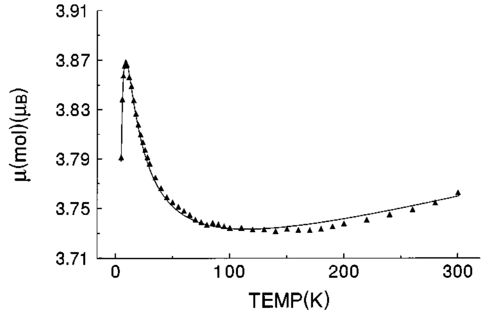

Figure 11. Variable temperature magnetic data for $[Cu_4(POAP\text{-}H)_4(H_2O)_2](ClO_4)_4\cdot 4H_2O$ (**1**). The solid line was calculated from eq 3 with $g = 2.124(2)$, $J = 7.28(9)$ cm^{-1}, $\rho = 0.0005$, $\theta = -3.4$ K, TIP = 220 × 10^{-6} emu (per mole), $10^2R = 0.16$ ($R = [\Sigma(\chi_{obs} - \chi_{calc})^2/\Sigma\chi^2_{obs}]^{1/2}$).

Variable temperature magnetic data for **4** show the familiar rise in μ on lowering the temperature, typical of intramolecular ferromagnetic behavior (Figure 12). An excellent data fit to eq

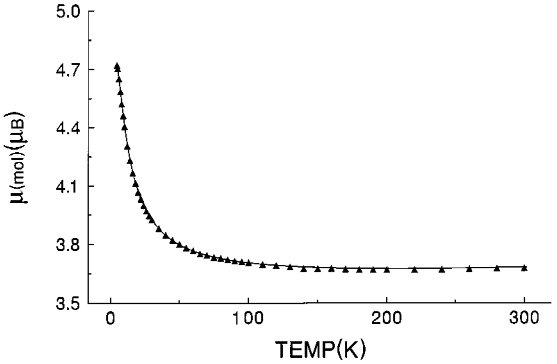

Figure 12. Variable temperature magnetic data for [Cu_4(6POAP-H)$_4$](ClO_4)$_4$ (**4**). The solid line was calculated from eq 3 with $g = 2.060(7)$, $J = 9.4(4)$ cm^{-1}, $\rho = 0.00004$, $\theta = -0.4$ K, TIP = 232×10^{-6} emu (per mole), $10^2R = 0.20$ ($R = [\Sigma(\chi_{obs} - \chi_{calc})^2/\Sigma\chi^2_{obs}]^{1/2}$).

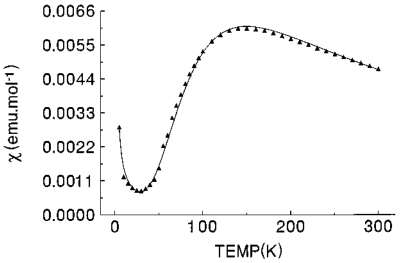

Figure 13. Variable temperature magnetic data for [Cu_4(POAP-H)$_4$(H_2O)$_2$] (NO_3)$_4$·4H_2O (**2**). The solid line was calculated from eq 3 with $g = 2.18(1)$, $J1 = -168(1)$ cm^{-1}, $J2 = 0$ cm^{-1}, $\rho = 0.029$, TIP = 240×10^{-6} emu (per mole), $10^2R = 0.29$ ($R = [\Sigma(\chi_{obs} - \chi_{calc})^2/\Sigma\chi^2_{obs}]^{1/2}$).

3 was obtained, even with the extremely small sample (7.87 mg). The solid line in the figure was calculated from the best fit data with $g = 2.060(7)$, $J = 9.4(4)$cm^{-1}, $\rho = 0.00004$, TIP = 232×10^{-6} emu (per mole), $\theta = -0.4$ K, $10^2R = 0.2$. The result is consistent with the ferromagnetism observed for this structural motif.

Compound **5** shows a very similar μ versus temperature profile, with an approximately constant value of 4.0 μ_B in the range of 300−100 K, and a sharp increase to 5.0 μ_B at 5 K. Fitting of the data to eq 3 gave $g = 2.221(5)$, $J = 8.2(4)$ cm^{-1}, $\rho = 0.0004$, TIP = 242×10^{-6} emu (per mole), $\theta = -0.4$ K, $10^2R = 1.1$. Again this compound fits the consistent pattern of intramolecular ferromagnetic exchange in these orthogonally bridged Cu_4O_4 square clusters.

Compound **2** is the odd man out in the series, and because of the trans diazine groups bridging the two pairs of copper centers via equatorial copper $d_{x^2-y^2}$ type magnetic orbitals, moderate antiferromagnetic coupling would be expected.[30−32] The variable temperature magnetic susceptibility data (Figure 13) show a broad maximum in χ_M at ≈140 K, consistent with intramolecular antiferromagnetic coupling. The data were fitted to an exchange expression (obtained from eqs 2, 3) derived from the Hamiltonian (eq 4) for four copper(II) centers in a rectangular arrangement. $J1$ represents the N−N exchange bridges and $J2$ the alkoxide exchange bridges. A good fit of

$$H = -\{J1(S_1 \cdot S_2 + S_3 \cdot S_4) + J2(S_2 \cdot S_3 + S_1 \cdot S_4)\} \qquad (4)$$

the data was obtained for $g = 2.18(1)$, $J1 = -168(1)$cm^{-1}, $J2 = 0$ cm^{-1}, $\rho = 0.029$, TIP = 240×10^{-6} emu (per mole), $10^2R = 0.29$. The solid line in Figure 13 was calculated with these parameters. This magnetic model is entirely consistent with the structure (Figure 1) which shows an orthogonal alkoxide bridging arrangement, and an almost trans bridging arrangement of the copper magnetic orbitals via the N−N bridge. As was shown previously[30−32] effective p orbital alignment within the N−N bridge leads to significant anti-ferromagnetic coupling between the copper centers.

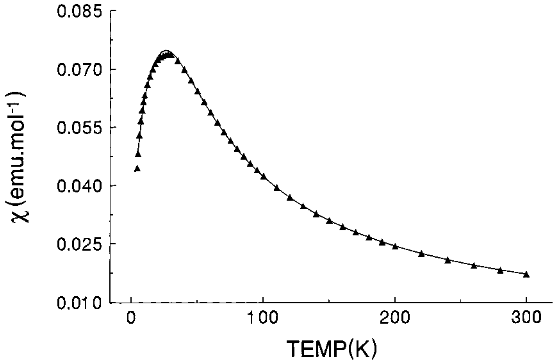

Figure 14. Variable temperature magnetic data for [Ni_4(POAP-H)$_4$(H_2O)$_4$](NO_3)$_4$·8H_2O (**6**). The solid line was calculated from eq 3 with $g = 2.29(1)$, $J = -13.6(2)$ cm^{-1}, $\rho = 0.012$, $\theta = 0$ K, TIP = 800×10^{-6} emu (per mole), $10^2R = 0.70$ ($R = [\Sigma(\chi_{obs} - \chi_{calc})^2/\Sigma\chi^2_{obs}]^{1/2}$).

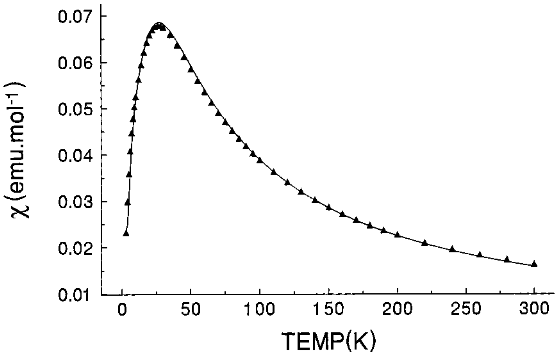

Figure 15. Variable temperature magnetic data for [Ni_4(PZOAP-H)$_4$(H_2O)$_4$](ClO_4)$_4$·5H_2O (**9**). The solid line was calculated from eq 3 with $g = 2.205(4)$, $J = -13.2(2)$ cm^{-1}, $\rho = 0.005$, $\theta = 0$ K, TIP = 800×10^{-6} emu (per mole), $10^2R = 0.35$ ($R = [\Sigma(\chi_{obs} - \chi_{calc})^2/\Sigma\chi^2_{obs}]^{1/2}$).

The variable temperature magnetic data for the square Ni_4O_4 complexes **6**−**9** show completely different behavior in comparison with the square Cu_4O_4 systems. A maximum is observed in the χ_M versus temperature profile in all cases, indicative of intramolecular antiferromagnetic coupling. **6** shows a maximum in χ_M at ~30 K (Figure 14). An excellent fit of the data to eq 3 ($S = 1$) was obtained with $g = 2.29(1)$, $J = -13.6(2)$ cm^{-1}, $\rho = 0.012$, TIP = 800×10^{-6} emu (per mole), $\theta = 0$ K, $10^2R = 0.7$. The solid line in Figure 14 was calculated with these parameters. The presence of antiferromagnetic exchange is entirely consistent with the structure, in which the four octahedral Ni(II) centers are bridged by alkoxide groups with Ni−O−Ni angles in the range 136.2−140.1°.[45] However, the observed J value is smaller than anticipated, based on the magnitude of the Ni−O−Ni angles,[45] and this may reflect the alternating short−long contact arrangement within the Ni_4O_4 square.

7 shows a similar χ_M versus temperature profile, with a maximum in χ_M at ~20 K, and an excellent fit of the data to eq 3 ($S = 1$) gave $g = 2.18(1)$, $J = -10.4(2)$ cm^{-1}, $\rho = 0.014$, $\theta = 0$ K, TIP = 800×10^{-6} emu (per mole), $10^2R = 0.9$. This is consistent with the square Ni_4O_4 structure of **7**. **9** has a room-temperature magnetic moment of 3.14 μ_B and shows a similar maximum in χ_M at 26 K (Figure 15), with an excellent fit of

---

(45) Nanda, K. K.; Thompson, L. K.; Bridson, J. N.; Nag, K. *J. Chem. Soc., Chem. Commun.* **1994**, 1337.

the data to eq 3 ($S = 1$) for $g = 2.205(4)$, $J = -13.2(2)$ cm^{-1}, $\rho = 0.005$, TIP = 800 × 10^{-6} emu (per mole), $10^2R = 0.35$. Compound **8** behaves in the same way, and a fit of the variable temperature susceptibility data to eq 3 ($S = 1$) gave $g = 2.28(1)$, $J = -15.9(3)$ cm^{-1}, $\rho = 0.029$, $\theta = 0$ K, TIP = 800 × 10^{-6} emu (per mole), $10^2R = 1.5$. The moderate antiferromagnetic coupling, comparable with **6**, **7**, and **9** suggests a similar structural motif with a Ni_4O_4 square structure. Visible absorption spectra (see experimental) for all the nickel complexes are very similar with ν_1 ($^3A_{2g} \rightarrow {}^3T_{2g}$) ($O_h$ symmetry) occurring at 964, 971, 970, and 994 nm for **6, 7**, **8**, and **9** respectively.

Conclusion

A series of polynucleating ligands with dual bridging functionality has been successfully used to generate predominantly a group of closely related square M_4O_4 complexes with copper(II) and nickel(II) salts, which arise through a self-assembly process, which is controlled in the sense that a predetermined structural arrangement is logically based on the strategic positions of the donor groups within the ligand backbone. In one unusual copper case a rectangular structure is produced, in which both N−N diazine and alkoxide bridge groups are involved. All of the square copper clusters exhibit intramolecular ferromagnetic spin exchange, associated with the orthogonal alkoxide bridging arrangement and the close proximity of the copper centers, while for the rectangular system the exchange is dominated by antiferromagnetic coupling via the N−N diazine bridge. All of the square nickel(II) complexes exhibit intramolecular antiferromagnetic coupling consistent with the alkoxide bridge structural arrangement.

Acknowledgment. We thank NSERC (Canada) and EPSRC (UK), and NATO for financial support for this study, and in particular NSERC for funding for the SQUID magnetometer.

Supporting Information Available: X-ray crystallographic files, in CIF format, for the structure determinations of $[Cu_4(POAP\text{-}H)_4(H_2O)_2](NO_3)_4{\cdot}4H_2O$ (**2**), $[Cu_4(POAPZ\text{-}H)_4(H_2O)](NO_3)_4{\cdot}3H_2O$ (**3**), $[Cu_4(6POAP\text{-}H)_4](ClO_4)_4$ (**4**), $[Cu_4(PZOAP\text{-}H)_4](NO_3)_4{\cdot}3H_2O$ (**5**), $[Ni_4(POAP\text{-}H)_4(H_2O)_4](NO_3)_4{\cdot}8H_2O$ (**6**), and $[Ni_4(PZOAP\text{-}H)_4(H_2O)_4](ClO_4)_4{\cdot}5H_2O$ (**9**). This material is available free of charge via the Internet at http://pubs.acs.org.

IC990598F